Chemistry–A European Journal
Full Paper
doi.org/10.1002/chem.202001483
Chemistry Europe
European Chemical Societies Publishing

Fluorescent Nanoparticles | *Hot Paper*

Fluorescent Metallacycle-Cored Amphiphilic Nanoparticles Formed by β-Cyclodextrin-Based Host–Guest Interactions towards Cancer Theranostics

Lingzhi Ma[+],[a] Tianfeng Yang[+],[b] Shuya Li[+],[c] Zeyuan Zhang,[a] Shuai Lu,[d, e] Ponmani Jeyakkumar,[a] Zhongxiao Song,[a] Xiaopeng Li,[d] Guocan Yu,[f] Dake Chu,*[g] Hang Liu,*[c] Yanmin Zhang,*[b] and Mingming Zhang*[a]

Abstract: Theranostic agents, taking the advantages of both imaging and therapeutic functions, are anticipated to be key components in the development of personalized medicine in which the therapeutic response can be real-time monitored. Herein, three metallacycles with pendent adamantane groups are prepared by coordination-driven self-assembly of Pt^{II} ligands with anticancer activities and tetraphenylethylene derivatives with emission. β-Cyclodextrin, which shows good host–guest interactions with adamantane moieties, was added to form amphiphilic supramolecular nanoparticles with the aim to enhance the aqueous solubilities and bioactivities of these metallacycles. Moreover, when rhodamine-modified β-cyclodextrin was used as the carrier, the release of the metallacycles from the nanoparticles could be monitored in situ through the fluorescence changes owing to the efficient fluorescence resonance energy transfer from the metallacycles to rhodamine-modified β-cyclodextrin. In vitro and in vivo studies showed that these nanoparticles not only served as cell imaging contrast agents but also displayed improved anticancer activities, allowing them to serve as potential candidates for cancer theranostics. This study provides a simple and efficient method to prepare theranostic agents by hierarchical supramolecular self-assembly, which will pave the way for image-guided cancer therapy, targeted cancer therapy, and related biomedical fields.

Introduction

Fluorescent supramolecular coordination complexes (SCCs) including metallacycles and metallacages have received considerable interest not only because of their appealing structures[1] but also owing to their broad applications in light-emitting materials, chemo-sensors, and biological agents.[2] The key feature of Pt^{II}-based fluorescent SCCs for diverse biomedical applications is the integration of Pt^{II} ligands with anticancer activities[3] and fluorescent ligands as bioimaging agents,[4] which makes them potential candidates for theranostic applications.[5] Compared with conventional fluorophores whose emission are (at least partially) quenched by the heavy atom effect after coordination,[6] the introduction of tetraphenylethylene (TPE) de-

[a] *L. Ma,[+] Dr. Z. Zhang, Dr. P. Jeyakkumar, Prof. Dr. Z. Song, Prof. Dr. M. Zhang*
State Key Laboratory for Mechanical Behavior of Materials
Shaanxi International Research Center for Soft Matter
School of Materials Science and Engineering
Xi'an Jiaotong University, Xi'an 710049 (P.R. China)
E-mail: mingming.zhang@xjtu.edu.cn

[b] *T. Yang,[+] Prof. Dr. Y. Zhang*
School of Pharmacy, Health Science Center
Xi'an Jiaotong University, Xi'an 710061 (P.R. China)
E-mail: zhang2008@mail.xjtu.edu.cn

[c] *S. Li,[+] Dr. H. Liu*
Division of Molecular Medicine
Hefei National Laboratory for Physical Sciences at Microscale
CAS Key Laboratory of Innate Immunity and Chronic Disease
School of Life Sciences
University of Science and Technology of China
Hefei 230027 (P.R. China)
E-mail: hangliu@ustc.edu.cn

[d] *S. Lu, Prof. Dr. X. Li*
College of Chemistry and Environmental Engineering
Shenzhen University
Shenzhen, Guangdong 518055 (P.R. China)

[e] *S. Lu*
College of Chemistry and Molecular Engineering, Zhengzhou University
Zhengzhou, Henan 450001 (P.R. China)

[f] *Dr. G. Yu*
Laboratory of Molecular Imaging and Nanomedicine
National Institute of Biomedical Imaging and Bioengineering
National Institutes of Health, Bethesda, MD 20892 (USA)

[g] *Dr. D. Chu*
Department of Gastroenterology
The First Affiliated Hospital of Xi'an Jiaotong University
Xi'an 710061 (P.R. China)
E-mail: chudake@xjtu.edu.cn

[+] *These authors contributed equally to this work.*

Supporting information and the ORCID identification number(s) for the author(s) of this article can be found under: https://doi.org/10.1002/chem.202001483.

rivatives enhances the fluorescence of derived SCCs because the restriction of the rotation of the aryl groups on TPE by the coordination bonds decreases the non-radiative decay.[7] Therefore, a series of TPE-based emissive metallacycles and metallacages were reported with diverse functions.[8] However, most fluorescent SCCs are hydrophobic, which makes them hard to be dissolved in physiological medium and limits their further biological applications. One strategy to solve this problem is to introduce amphiphilic polymers to encapsulate these SCCs and deliver them to the specific position.[9] For example, Stang et al. linked an amphiphilic polymer to the metalacyclic structure and combined the cytotoxicity of doxorubicin and Pt^{II} metallacycles to achieve a synergistic anticancer effect.[9a] Huang, Cook, and co-workers introduced photodynamic therapy to increase the anticancer efficacy of Pt^{II} metallacycles.[9c] However, this method greatly reduces the content of SCCs in the system, and thus combinational therapy is required to improve the therapeutic efficacy. Therefore, these SCC-based theranostic systems are complicated and the release of the metallacycles from these complexes is difficult to monitor.

As water-soluble macrocycles, cyclodextrins (CDs)[10] possess the ability to encapsulate hydrophobic guests within their cavities. As such, they have been widely used as pharmaceutical excipients with good biocompatibility to improve the solubility and bioavailability of drugs.[11] Moreover, CDs can be easily modified by introducing other functional groups, such as targeted ligands or fluorophores to deliver more functions.[12] Inspired by this, adamantane moieties, excellent guests for β-CD,[13] were introduced into fluorescent metallacyclic structures to form adamantane appendant metallacycles. The addition of β-CD into the metallacycles formed amphiphilic nanoparticles, which were further used as cancer theranostic agents. The introduction of β-CD not only enhanced the solubility of the metallacycles through host–guest interactions with the pendent adamantane groups[10,13] but also increased the anticancer activity by the formation of nanoparticles with enhanced permeability and retention (EPR) effect.[14] Moreover, to monitor the release of the metallacycles in situ to ensure therapeutic efficacy and safety, a rhodamine-modified β-CD (**RDM-β-CD**)[15] was prepared and used as the carrier for the metallacycles. Owing to the good spectral overlap between the emission of the metallacycles and the absorption of **RDM-β-CD**, efficient fluorescence resonance energy transfer (FRET)[16] took place from the metallacycles to **RDM-β-CD**. It is anticipated that the fluorescence of the metallacycles would be recovered after being released from the supramolecular nanoparticles, which can be used to monitor their release process in real time.

Results and Discussion

Preparation and characterization of materials

The syntheses of metallacycles and the preparation of amphiphilic nanoparticles are shown in Scheme 1. Esterification of precursor **1**[5a] with 1-adamantanecarbonyl chloride gave intermediate **2**, which was reacted with pydine-4-boronic acid to afford the dipyridyl donor **3** by the Suzuki reaction. By stirring ligand **3** and the corresponding platinum acceptors **4a–c** in dichloromethane at room temperature for 12 h, metallacycles **5a–c** were obtained in nearly quantitative yield. The addition of metallacycles **5a–c** into an aqueous solution of β-CD or **RDM-β-CD** formed amphiphilic supramolecular nanoparticles **6a–c** or **7a–c** (β-CD/adamantane = 1:1 in molar ratio), respectively.

Metallacycles **5a–c** were well characterized by multinuclear NMR ($^{31}P\{^1H\}$ and ^1H) analysis and electrospray ionization time-of-flight mass spectrometry (ESI-TOF-MS) (see the Supporting Information for details), which suggest their correct chemical structures. The UV/Vis absorption and fluorescence spectra of ligand **3**, metallacycles **5a–c**, and supramolecular nanoparticles **6a–c** in 1% DMSO/water are shown in Figure 1.[17] Ligand **3** displays two absorption bands centered at 257 nm and 328 nm with molar absorption coefficients (ε) of 2.92×10^4 and $2.21\times10^4\,M^{-1}cm^{-1}$, respectively (Figure 1a). Upon the formation of metallacycles **5a–c**, their absorption increased owing to the incorporation of multiple ligands into one metallacyclic structure. Metallacycle **5a** shows three absorption bands centered at 260, 284, and 318 nm with $\varepsilon = 1.59\times10^5$, 9.78×10^4, and $8.83\times10^4\,M^{-1}cm^{-1}$, respectively. There are two distinct bands for metallacycles **5b** and **5c** centered at 257 and 325 nm with $\varepsilon = 7.50\times10^4$ and $4.79\times10^4\,M^{-1}cm^{-1}$ for **5b** and 1.36×10^5, $1.78\times10^5\,M^{-1}cm^{-1}$ for **5c**, respectively. Nanoparticles **6a–c** show very similar absorption bands with those of metallacycles **5a–c** owing to the weak absorption for β-CD. All these species are emissive in 1% DMSO/water (Figure 1b) with maximum emission at approximately 500 nm because water is a poor solvent for them, thus making them aggregate to give bright emission.[7] This characteristic indicates that they could be used as cell imaging contrast agents in aqueous solution.

To study how the addition of β-CD increases the solubilities of metallacycles **5a–c** in water, phase solubility diagrams[18] (Figure S14 in the Supporting Information) were recorded. As the concentration of β-CD increases, the solubilities of all the three metallacycles are enhanced. Especially for metallacycle **5b**, its solubility increased to $1.2\,g\,L^{-1}$ in 10 mM β-CD solution. The size and morphology of nanoparticles **6a–c** were studied by dynamic light scattering (DLS) and scanning electron microscopy (SEM). DLS (Figure 1c) shows that the average hydrodynamic diameters of nanoparticles **6a**, **6b**, and **6c** are 24.04, 27.65, and 22.41 nm, respectively. SEM images indicate that these nanoparticles are micellar structures with diameters of 20–30 nm (Figure S15 in the Supporting Information), which is consistent with the DLS results. The size distribution of these nanoparticles is wide, indicating that these amphiphilic structures can easily aggregate in aqueous solution. It is worth mentioning that no significant size or absorption changes were observed for these nanoparticles after 7 days (Figure S16 in the Supporting Information), indicating that they are stable in aqueous solutions. It is believed that nanoparticles in this size range show an EPR effect,[14] which can enhance their uptake and retention by tumors, thus increasing their anticancer efficacy.

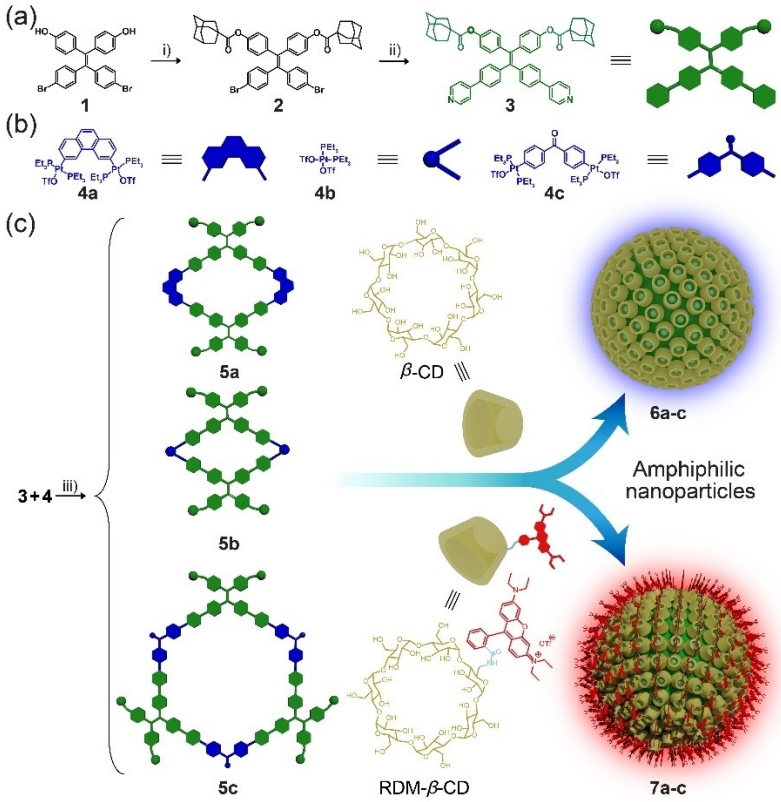

Scheme 1. Synthetic routes, chemical structures, and cartoon representations of compounds used in this study. (a) Synthesis of dipyridyl donor **3**. (b) Chemical structures and cartoon representations of diplatinum acceptors **4a–c**. (c) Self-assembly of metallacycles **5a–c** and amphiphilic nanoparticles **6a–c** and **7a–c**. Conditions: i) 1-adamantanecarbonyl chloride, Et_3N, CH_2Cl_2, room temperature, 12 h; 85%; ii) pyridine-4-boronic acid, K_2CO_3, $Pd(PPh_3)_4$, tetrabutylammonium bromide, toluene/ethanol/water (4:1:1), reflux, 48 h; 56%; iii) CH_2Cl_2, room temperature, 12 h; 100%.

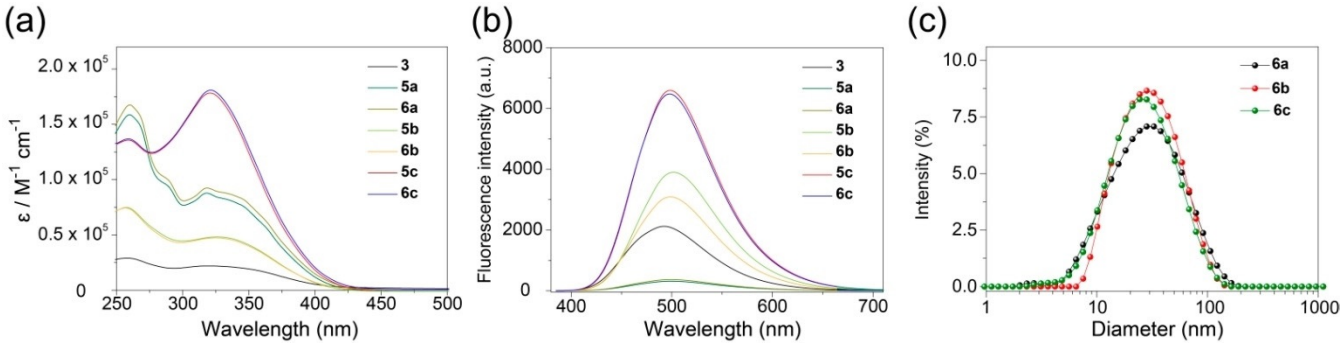

Figure 1. (a) UV/Vis absorption and (b) emission spectra of all the compounds in 1% DMSO in H_2O. (c) Particle size distributions of amphiphilic nanoparticles **6a–c** measured by DLS. λ_{ex} = 365 nm, c = 10 μM.

Cell imaging

The applications of nanoparticles **6a–c** for bioimaging were investigated by confocal laser scanning microscopy (CLSM) in cervical cancer HeLa cells and non-small cell lung cancer A549 cells. The cells are stained by FITC and nanoparticles **6a–c** simultaneously and photos (Figure 2) were taken 6 h after incubation. Based on the merged figures, bright blue fluorescence derived from these nanoparticles was observed in the cytoplasm of the cells,[5a] suggesting that these nanoparticles could be used as contrast agents for cell imaging.

It is a challenge to monitor the release of the reagents in situ in drug delivery systems. In our system, the fluorescent feature of these nanoparticles offers a pathway to use the emission changes to monitor this process. To improve the accuracy and precision, **RDM-β-CD** instead of β-CD was prepared and used as the carrier to prepare nanoparticles **7a–c** with dual emission. Because the emission of the metallacycles **5a–c** overlaps well with the absorption of **RDM-β-CD** (Figure 3a and Figure S20 in the Supporting Information), efficient FRET took place from the metallacycles **5a–c** to **RDM-β-CD**. This process was proved by fluorescence titration experiments (Figure 3b

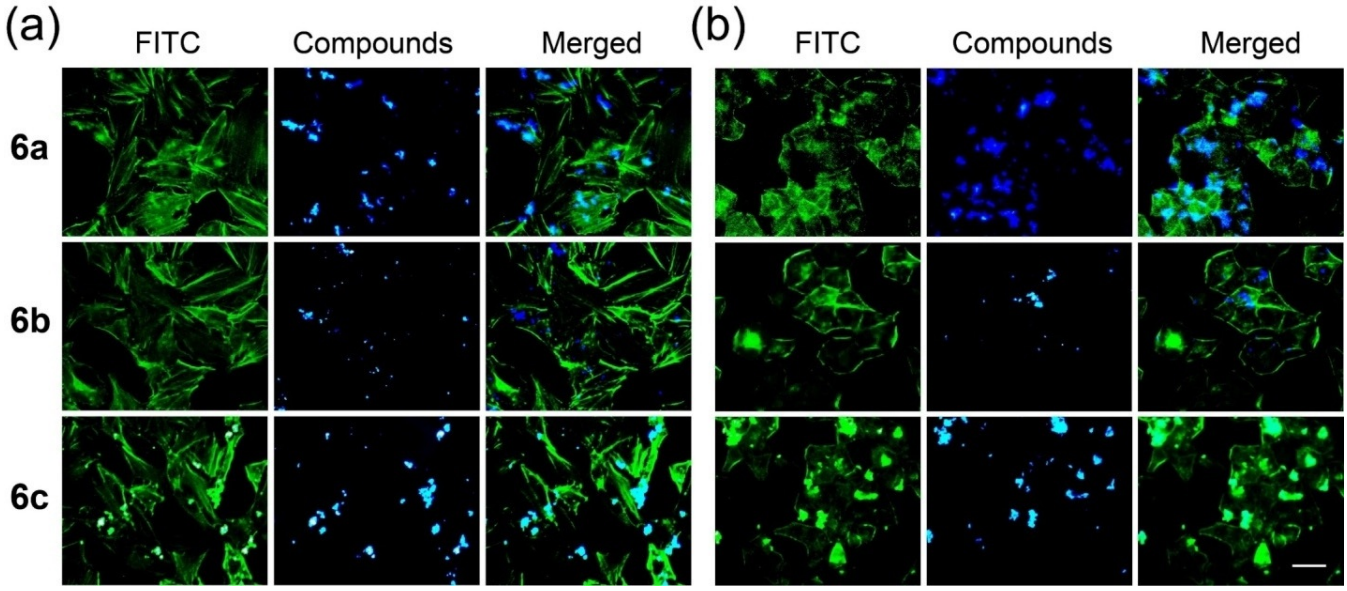

Figure 2. CLSM images of (a) A549 and (b) HeLa cells after the incubation with FITC and nanoparticles **6a**, **6b**, or **6c**. The scale bar is 30 μm.

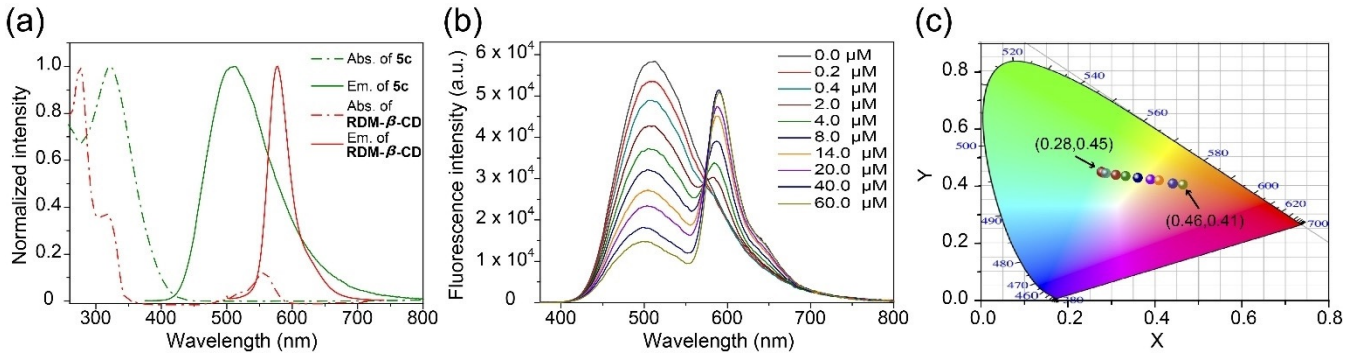

Figure 3. FRET between metallacycle **5c** and **RDM-β-CD**. (a) Absorption and emission spectra of metallacycle **5c** and **RDM-β-CD**. (b) Emission of the solution of metallacycle **5c** with increasing concentrations of **RDM-β-CD**. (c) CIE diagram of metallacycle **5c** with different concentrations of **RDM-β-CD**. $c = 10$ μM for metallacycle **5c**, and $\lambda_{ex} = 365$ nm.

and Figure S21 in the Supporting Information). For example, with the addition of **RDM-β-CD** into the aqueous solution of metallacycle **5c**, the emission centered at approximately 500 nm derived from metallacycles decreased whereas the emission at approximately 590 nm from RDM increased. Correspondingly, the color of the solution changed from green to yellow, as seen from the Commission internationale de l'éclairage (CIE) diagram (Figure 3c). A similar phenomenon was also observed for metallacycles **5a** and **5b** (Figure S21 in the Supporting Information). The dramatic color change makes it possible to monitor the release of the metallacycles from the nanoparticles in cells.

To monitor the release process in cancer cells, the HeLa cells were incubated with the amphiphilic nanoparticles **7a–c** and the images of the cells (Figure 4a–c) were taken by CLSM after different incubation times. After 1 h of incubation, only very weak red fluorescence derived from **RDM-β-CD** was observed owing to the insufficient cell uptake. Up to 3 h later, clear red fluorescence was seen whereas nearly no blue fluorescence derived from the metallacycles was observed, indicating that the fluorescence of the metallacycles was quenched by FRET and few metallacycles were released from the nanoparticles at this time. After 6 h of incubation, the blue fluorescence from the metallacycles emerged, suggesting the release of the metallacycles from the nanoparticles to cells, and more intense blue fluorescence was observed after 8 h of incubation. The fluorescence intensity at different incubation times was further investigated by using a microplate reader (Figure 4d–f). The fluorescence intensity of **RDM-β-CD** reached a maximum after 6 h of incubation, indicating that the cellular uptake of the nanoparticles reached an equilibrium state at this time. However, the emission derived from metallacycles kept increasing as time went by, which is due to the continuous release of the metallacycles from nanoparticles. These results were also consistent with those obtained by flow cytometry analysis (Figure 4g–i). In the beginning (1 h after incubation), only 10% cells were observed with red fluorescence. As the incubation time was prolonged, 80–90% cells exhibited red fluorescence and mod-

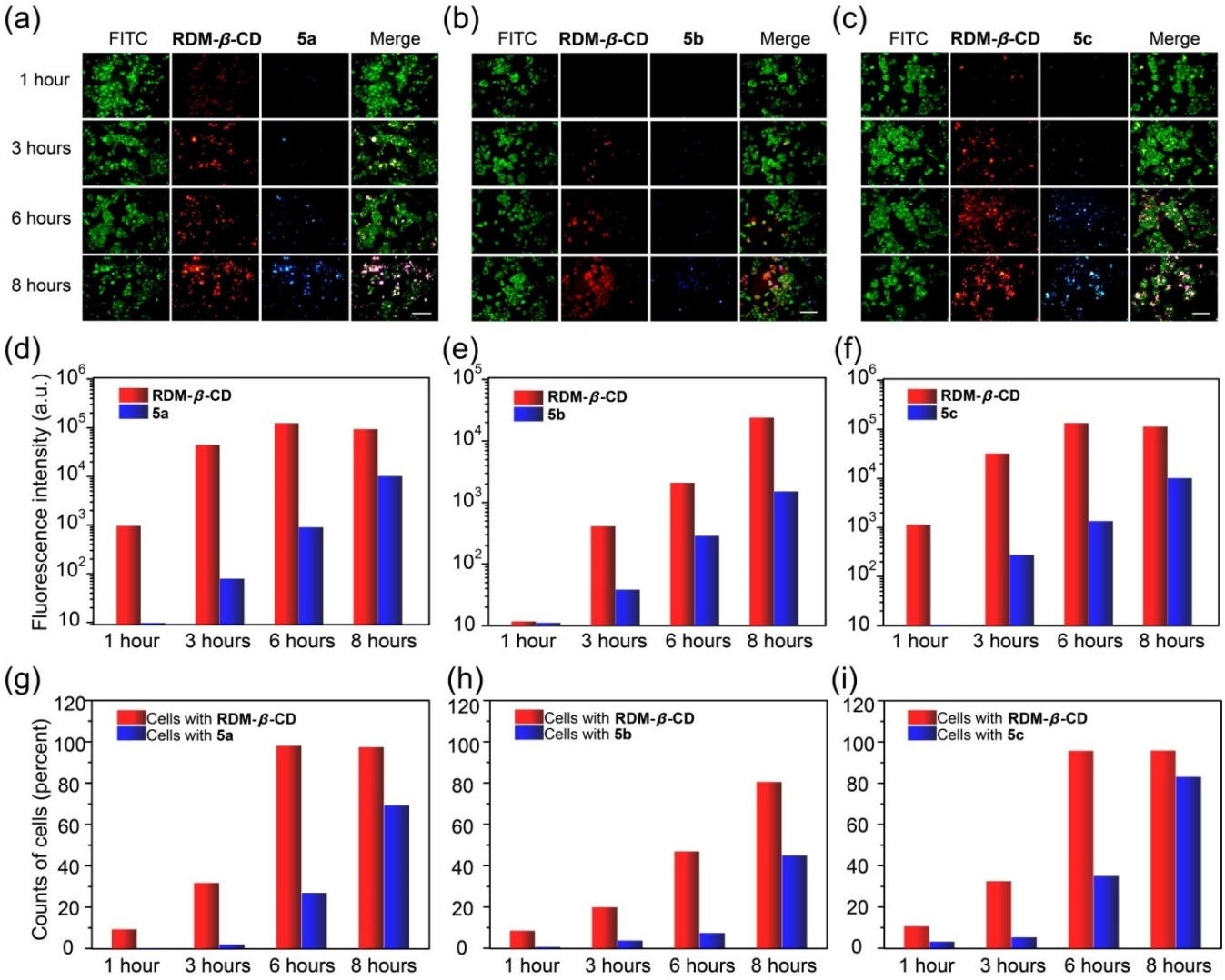

Figure 4. (a–c) CLSM images of HeLa cells after incubation with amphiphilic nanoparticles **7a–c** at different times. The scale bar is 100 μm. (d–f) Fluorescence intensity of HeLa cells incubated with amphiphilic nanoparticles **7a–c** at different times. (g–i) Counts of cells with emission of metallacycles **5a–c** or **RDM-β-CD** at different incubation times.

erate blue fluorescence was observed after 6 h of incubation owing to the release of the metallacycles from the nanoparticles. The fluorescence changes offered a visual method to monitor the release of the metallacycles from the nanoparticles.

Anticancer study

The anticancer activities of metallacycles **5a–c** and nanoparticles **6a–c** against five human cancer cell lines (non-small cell lung, cervical, hepatocellular, colorectal, and breast cancer cells) were evaluated by MTT (3-(4′,5′-dimethylthiazol-2′-yl)-2,5-diphenyltetrazolium bromide) assay. The IC_{50} values of all the species are shown in Table 1. The nanoparticles **6a–c** and the metallacycles **5a–c** showed considerable anticancer activities against all the tested cells and the IC_{50} values of nanoparticles **6a–c** are slightly lower than those of metallacycles **5a–c**, indicating that the addition of β-CD enhances the anticancer activities, as reported in some clinical drugs.[11] It is worth mentioning that **6a** and **6c** show much higher cytotoxicity than **6b**, which is probably because the aromatic platinum ligands could form more stable complexes with DNA chains, resulting in more strongly disturbed replication and transcription process of DNA.[19] Unsurprisingly, the DNA quantities of HeLa and A549 cells after incubating with **6a** or **6c** were significantly reduced (Figure S28 in the Supporting Information), which further verified the assumption.

In vivo experiments (Figure 5) were further conducted to evaluate the theranostic activities of metallacycles **5a–c** and nanoparticles **6a–c**. HeLa tumor-bearing nude mice with a subcutaneous xenograft tumor models were used for the study. The in vivo tracking imaging of mice after intratumoral injection of these compounds was first performed to study the uptake of the amphiphilic nanoparticles **6a–c**. A significant number of nanoparticles accumulated in the tumor area 6 h post injection (Figure 5a and Figure S29 in the Supporting In-

Table 1. IC_{50} values of metallacycles **5a–c** and nanoparticles **6a–c** towards different cell lines.

Cell types	Cell lines	IC_{50} [μM]					
		5a	**6a**	**5b**	**6b**	**5c**	**6c**
non-small cell lung cancer	A549	11.26	8.98	22.10	18.92	8.91	7.42
cervical cancer	HeLa	9.57	8.21	25.23	22.83	7.83	5.99
hepatocellular cancer	SMMC-7721	8.94	7.33	24.70	20.21	9.91	7.09
colorectal cancer	LoVo	19.42	18.29	–[a]	–[a]	19.27	18.99
breast cancer	MDA-MB-231	20.05	17.53	–[a]	–[a]	18.45	16.05

[a] "–" means that it is not suitable to calculate the IC_{50} values.

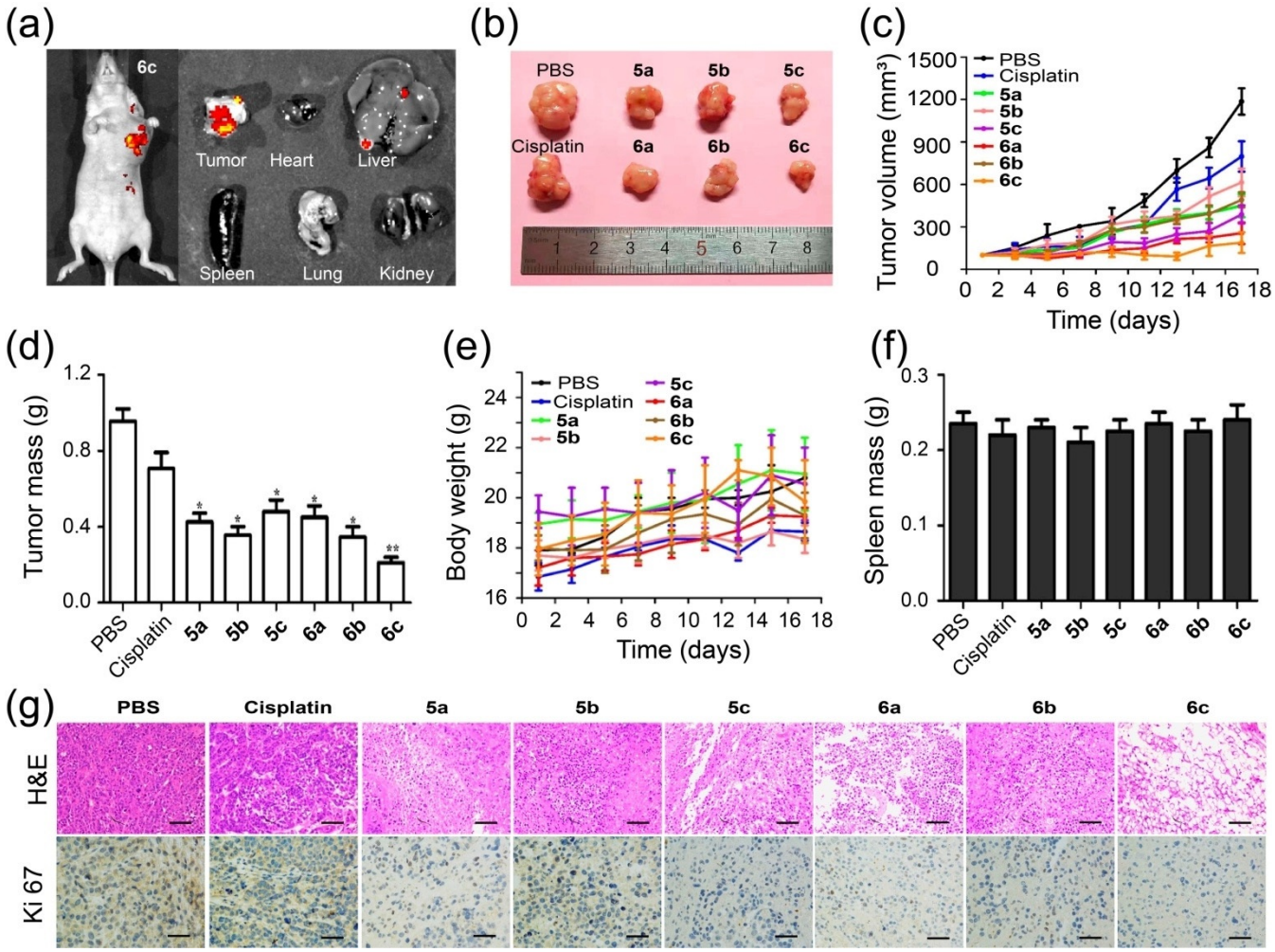

Figure 5. (a) Images of a mouse and its different organs after intratumoral injection of **6c**. (b) Images of the orthotopic tumors harvested from the mice treated with different formulations. (c) Tumor volume changes, (d) tumor mass, (e) body weight changes, and (f) spleen mass after treatments. (g) H&E and Ki-67 staining of the tumor tissues from each group. The scale bar is 200 μm and 50 μm for H&E and histological examination, respectively.

formation), indicating that these nanoparticles showed long-term fluorescence and possessed good tumor accumulation and retention capabilities.

The in vivo antitumor performance of the nanoparticles was further evaluated. The mice with tumors were intratumorally injected with PBS buffer, cisplatin, metallacycles **5a–c**, and nanoparticles **6a–c** in a dose of 2 mg kg^{-1} in platinum weight. The average tumor size of the different groups was monitored for 2 weeks to evaluate the therapeutic effect. All the test species including metallacycles **5a–c** and nanoparticles **6a–c** showed better antitumor activities than cisplatin, as evidenced by the size of the tumor after treatment (Figure 5b). Nanoparticles **6c** exhibited the best antitumor properties as confirmed by the smallest tumor volume (Figure 5b), which agreed well with the tumor volume (Figure 5c) and tumor mass (Figure 5d) measurements. The body weights of the mice are very similar (Figure 5e) and the spleen mass (Figure 5f) remained almost constant, suggesting that these nanoparticles can be used as

therapeutic agents for cancer treatment. H&E staining analysis showed clear shrinkage and changes of the tumor cells in all the test species, suggesting their effective antitumor activities (Figure 5g). Furthermore, all the test species exhibited clear inhibitory effect on tumor proliferation in immunohistochemical staining of Ki-67 (Figure 5g).

Conclusion

Three metallacycles with pendant adamantane groups were successfully prepared and further used to prepare amphiphilic nanoparticles through β-CD-based host–guest interactions. The introduction of β-CD into these nanoparticles increases the solubilities of the metallacycles in water, and thus leading to enhanced bioavailability and cell uptake efficiency. These nanoparticles performed as good contrast agents for cell imaging owing to their good fluorescence derived from the TPE luminogens. The release of the metallacycles from the nanoparticles could be monitored in situ through the fluorescence changes because of the FRET from the metallacycles to **RDM-β-CD**. Moreover, they showed better anticancer activities than sole metallacycles and cisplatin, as evidenced by their IC_{50} values as well as in vivo study. This study not only provides an efficient method to improve the theranostic properties of Pt^{II} metallacycles by host–guest chemistry, but also gives a strategy to track the release of the metallacycles from the system by the FRET process, which will be beneficial for the development of supramolecular theranostics.

Acknowledgments

This work was supported by the National Natural Science Foundation of China (21801203 to M.Z., 81773772 to Y.Z., and 81672460 to D.C.), and The Key Research and Development Program of Shaanxi Province (2019KW-019 to M.Z. and 2019SF-012 to D.C.). M.Z. is thankful for start-up funds from Xi'an Jiaotong University. We thank Dr. Gang Chang and Yu Wang at the Instrument Analysis Center and Dr. Aqun Zheng and Junjie Zhang at Experimental Chemistry Center of Xi'an Jiaotong University for NMR and fluorescence measurements. We also acknowledge the mass spectrometry characterization by Molecule Scale Lab.

Conflict of interest

The authors declare no conflict of interest.

Keywords: fluorescence · host–guest interactions · metal coordination · self-assembly · theranostics

[1] a) T. R. Cook, Y. R. Zheng, P. J. Stang, *Chem. Rev.* **2013**, *113*, 734–777; b) A. M. Lifschitz, M. S. Rosen, C. M. McGuirk, C. A. Mirkin, *J. Am. Chem. Soc.* **2015**, *137*, 7252–7261; c) A. J. McConnell, C. S. Wood, P. P. Neelakandan, J. R. Nitschke, *Chem. Rev.* **2015**, *115*, 7729–7793; d) T. R. Cook, P. J. Stang, *Chem. Rev.* **2015**, *115*, 7001–7045; e) H. Takezawa, S. Akiba, T. Murase, M. Fujita, *J. Am. Chem. Soc.* **2015**, *137*, 7043–7046; f) M. Yamashina, M. M. Sartin, Y. Sei, M. Akita, S. Takeuchi, T. Tahara, M. Yoshizawa, *J. Am. Chem. Soc.* **2015**, *137*, 9266–9269; g) H. Sepehrpour, W. Fu, Y. Sun, P. J. Stang, *J. Am. Chem. Soc.* **2019**, *141*, 14005–14020.

[2] a) K. L. Haas, K. J. Franz, *Chem. Rev.* **2009**, *109*, 4921–4960; b) M. Schulze, V. Kunz, P. D. Frischmann, F. A. Würthner, *Nat. Chem.* **2016**, *8*, 576–583; c) M. L. Saha, X. Yan, P. J. Stang, *Acc. Chem. Res.* **2016**, *49*, 2527–2539; d) J. Rodríguez, J. Mosquera, J. R. Couceiro, J. R. Nitschke, M. E. Vázquez, J. L. Mascareñas, *J. Am. Chem. Soc.* **2017**, *139*, 55–58; e) C. B. Huang, L. Xu, J. L. Zhu, Y. X. Wang, B. Sun, X. Li, H. B. Yang, *J. Am. Chem. Soc.* **2017**, *139*, 9459–9462; f) A. J. Musser, P. P. Neelakandan, J. M. Richter, H. Mori, R. H. Friend, J. R. Nitschke, *J. Am. Chem. Soc.* **2017**, *139*, 12050–12059; g) M. Zhang, S. Yin, J. Zhang, Z. Zhou, M. L. Saha, C. Lu, P. J. Stang, *Proc. Natl. Acad. Sci. USA* **2017**, *114*, 3044–3049.

[3] a) T. C. Johnstone, K. Suntharalingam, S. J. Lippard, *Chem. Rev.* **2016**, *116*, 3436–3486; b) X. Wang, X. Wang, S. Jin, N. Muhammad, Z. Guo, *Chem. Rev.* **2019**, *119*, 1138–1192.

[4] a) D. Ding, K. Li, B. Liu, B. Z. Tang, *Acc. Chem. Res.* **2013**, *46*, 2441–2453; b) L. Y. Niu, Y. Z. Chen, H. R. Zheng, L. Z. Wu, C. H. Tung, Q. Z. Yang, *Chem. Soc. Rev.* **2015**, *44*, 6143–6160; c) D. Wu, A. C. Sedgwick, T. Gunnlaugsson, E. U. Akkaya, J. Yoon, T. D. James, *Chem. Soc. Rev.* **2017**, *46*, 7105–7123; d) H. B. Cheng, Y. Li, B. Z. Tang, J. Yoon, *Chem. Soc. Rev.* **2020**, *49*, 21–31.

[5] a) M. Zhang, S. Li, X. Yan, Z. Zhou, M. L. Saha, Y. C. Wang, P. J. Stang, *Proc. Natl. Acad. Sci. USA* **2016**, *113*, 11100–11105; b) G. Yu, T. R. Cook, Y. Li, X. Yan, D. Wu, L. Shao, J. Shen, G. Tang, F. Huang, X. Chen, P. J. Stang, *Proc. Natl. Acad. Sci. USA* **2016**, *113*, 13720–13725; c) L. Ma, T. Yang, Z. Zhang, S. Yin, Z. Song, W. Shi, D. Chu, Y. Zhang, M. Zhang, *Chin. Chem. Lett.* **2019**, *30*, 1942–1946; d) P. Jeyakkumar, Y. Liang, M. Guo, S. Lu, D. Xu, X. Li, B. Guo, G. He, D. Chu, M. Zhang, *Angew. Chem. Int. Ed.* **2020**, *59*, 15199–15203; *Angew. Chem.* **2020**, *132*, 15311–15315; e) X. Wang, Q. Su, Z. Zhang, J. Yang, Y. Zhang, M. Zhang, *Chem. Commun.* **2020**, *56*, 8460–8463.

[6] a) Z. Li, N. Kishi, K. Hasegawa, M. Akita, M. Yoshizawa, *Chem. Commun.* **2011**, *47*, 8605–8607; b) X. Yan, P. Wei, Y. Liu, M. Wang, C. Chen, J. Zhao, G. Li, M. L. Saha, Z. Zhou, Z. An, X. Li, P. J. Stang, *J. Am. Chem. Soc.* **2019**, *141*, 9673–9679.

[7] a) Z. Zhao, J. W. Y. Lam, B. Z. Tang, *J. Mater. Chem.* **2012**, *22*, 23726–23740; b) J. Mei, Y. Hong, J. W. Y. Lam, A. Qin, Y. Tang, B. Z. Tang, *Adv. Mater.* **2014**, *26*, 5429–5479; c) J. Mei, N. L. Leung, R. T. Kwok, J. W. Lam, B. Z. Tang, *Chem. Rev.* **2015**, *115*, 11718–11940.

[8] a) X. Yan, T. R. Cook, P. Wang, F. Huang, P. J. Stang, *Nat. Chem.* **2015**, *7*, 342–348; b) M. Zhang, M. L. Saha, M. Wang, Z. Zhou, B. Song, C. Lu, X. Yan, X. Li, F. Huang, S. Yin, P. J. Stang, *J. Am. Chem. Soc.* **2017**, *139*, 5067–5074; c) Z. Zhang, Z. Zhao, Y. Hou, H. Wang, X. Li, G. He, M. Zhang, *Angew. Chem. Int. Ed.* **2019**, *58*, 8862–8866; *Angew. Chem.* **2019**, *131*, 8954–8958; d) L. Chen, C. Chen, Y. Sun, S. Lu, H. Huo, T. Tan, A. Li, X. Li, G. Ungar, F. Liu, M. Zhang, *Angew. Chem. Int. Ed.* **2020**, *59*, 10143–10150; *Angew. Chem.* **2020**, *132*, 10229–10236.

[9] a) G. Yu, M. Zhang, M. L. Saha, Z. Mao, J. Chen, Y. Yao, Z. Zhou, Y. Liu, C. Gao, F. Huang, X. Chen, P. J. Stang, *J. Am. Chem. Soc.* **2017**, *139*, 15940–15949; b) G. Yu, S. Yu, M. L. Saha, J. Zhou, T. R. Cook, B. C. Yung, J. Chen, Z. Mao, F. Zhang, Z. Zhou, Y. Liu, L. Shao, S. Wang, C. Gao, F. Huang, P. J. Stang, X. Chen, *Nat. Commun.* **2018**, *9*, 4335; c) J. Zhou, Y. Zhang, G. Yu, M. R. Crawley, C. R. P. Fulong, A. E. Friedman, S. Sengupta, J. Sun, Q. Li, F. Huang, T. R. Cook, *J. Am. Chem. Soc.* **2018**, *140*, 7730–7736; d) Y. Sun, F. Ding, Z. Zhou, C. Li, M. Pu, Y. Xu, Y. Zhan, X. Lu, H. Li, G. Yang, Y. Sun, P. J. Stang, *Proc. Natl. Acad. Sci. USA* **2019**, *116*, 1968–1973; e) Y. Qin, L. J. Chen, F. Dong, S. T. Jiang, G. Q. Yin, X. Li, Y. Tian, H. B. Yang, *J. Am. Chem. Soc.* **2019**, *141*, 8943–8950.

[10] G. Crini, *Chem. Rev.* **2014**, *114*, 10940–10975.

[11] M. E. Davis, M. E. Brewster, *Nat. Rev. Drug Discovery* **2004**, *3*, 1023–1035.

[12] a) F. Bellia, D. La Mendola, C. Pedone, E. Rizzarelli, M. Saviano, G. Vecchio, *Chem. Soc. Rev.* **2009**, *38*, 2756–2781; b) J. Zhou, H. Ritter, *Polym. Chem.* **2010**, *1*, 1552–1559; c) G. Chen, M. Jiang, *Chem. Soc. Rev.* **2011**, *40*, 2254–2266; d) A. Harada, Y. Takashima, M. Nakahata, *Acc. Chem. Res.* **2014**, *47*, 2128–2140; e) J. Zhou, G. Yu, F. Huang, *Chem. Soc. Rev.* **2017**, *46*, 7021–7053; f) Y. Chen, F. H. Huang, Z. T. Li, Y. Liu, *Sci. China Chem.* **2018**, *61*, 979–992; g) G. Yu, X. Chen, *Theranostics* **2019**, *9*, 3041–3073.

[13] B. V. K. J. Schmidt, C. Barner-Kowollik, *Angew. Chem. Int. Ed.* **2017**, *56*, 8350–8369; *Angew. Chem.* **2017**, *129*, 8468–8488.

[14] H. Maeda, *Bioconjugate Chem.* **2010**, *21*, 797–802.

[15] M. Malanga, L. Jicsinszky, É. Fenyvesi, *J. Drug Del. Sci. Tech.* **2012**, *22*, 260 – 265.
[16] a) H. Q. Peng, L. Y. Niu, Y. Z. Chen, L. Z. Wu, C. H. Tung, Q. Z. Yang, *Chem. Rev.* **2015**, *115*, 7502 – 7542; b) R. F. Wang, H. Q. Peng, P. Z. Chen, L. Y. Niu, J. F. Gao, L. Z. Wu, C. H. Tung, Y. Z. Chen, Q. Z. Yang, *Adv. Funct. Mater.* **2016**, *26*, 5419 – 5425; c) X. Guo, L. Wang, K. Duval, J. Fan, S. Zhou, Z. Chen, *Adv. Mater.* **2018**, *30*, 1705436; d) Z. Zhang, Z. Zhao, L. Wu, S. Lu, S. Ling, G. Li, L. Xu, L. Ma, Y. Hou, X. Wang, X. Li, G. He, K. Wang, B. Zou, M. Zhang, *J. Am. Chem. Soc.* **2020**, *142*, 2592 – 2600.
[17] Here, we used 1% DMSO/water as the solvent for better comparison. Although the nanoparticles **6a–c** can be dispersed well in water, the solubilities of ligand **3** and metallacycles **5a–c** are not good, so 1% DMSO was added to dissolve all the species.
[18] D. Ma, G. Hettiarachchi, D. Nguyen, B. Zhang, J. B. Wittenberg, P. Y. Zavalij, V. Briken, L. Isaacs, *Nat. Chem.* **2012**, *4*, 503 – 510.
[19] a) A. Basu, S. Krishnamurthy, *J. Nucleic Acids* **2010**, 201367; b) J. Hu, J. D. Lieb, A. Sancar, S. Adar, *Proc. Natl. Acad. Sci. USA* **2016**, *113*, 11507 – 11512.

Manuscript received: March 27, 2020
Revised manuscript received: May 6, 2020
Accepted manuscript online: May 19, 2020
Version of record online: September 11, 2020